IEEE TRANSACTIONS ON VISUALIZATION AND COMPUTER GRAPHICS, VOL. 14, NO. 4, JULY/AUGUST 2008, PP. 756-771

Data-Driven Visualization and Group Analysis of Multichannel EEG Coherence with Functional Units

Michael ten Caat[(a,b)], Natasha M. Maurits[(b,c)], and Jos B. T. M. Roerdink[(a,b)], *Senior Member, IEEE*

***Abstract*— A typical data-driven visualization of electroencephalography (EEG) coherence is a graph layout, with vertices representing electrodes and edges representing significant coherences between electrode signals. A drawback of this layout is its visual clutter for multichannel EEG. To reduce clutter, we define a functional unit (FU) as a data-driven region of interest (ROI). An FU is a spatially connected set of electrodes recording pairwise significantly coherent signals, represented in the coherence graph by a spatially connected clique. Earlier we presented two methods to detect FUs, a maximal clique based (MCB) method (time complexity $O(3^{n/3})$, with n the number of vertices) and a more efficient watershed based (WB) method (time complexity $O(n^2 \log n)$). To reduce the potential over-segmentation of the WB method, we introduce an improved watershed based (IWB) method (time complexity $O(n^2 \log n)$). The IWB method merges basins representing FUs during the segmentation if they are spatially connected and if their union is a clique. The WB and IWB method both are up to a factor of 100,000 faster than the MCB method for a typical multichannel setting with 128 EEG channels, thus making interactive visualization of multichannel EEG coherence possible. Results show that, considering the MCB method as the gold standard, the difference between IWB and MCB FU maps is smaller than between WB and MCB FU maps. We also introduce two novel group maps for data-driven group analysis as extensions of the IWB method. First, the group mean coherence map preserves dominant features from a collection of individual FU maps. Second, the group FU size map visualizes the average FU size per electrode across a collection of individual FU maps. Finally, we employ an extensive case study to evaluate the IWB FU map and the two new group maps for data-driven group analysis. Results, in accordance with conventional findings, indicate differences in EEG coherence between younger and older adults. However, they also suggest that an initial selection of hypothesis-driven ROIs could be extended with additional data-driven ROIs.**

***Index Terms*— Information visualization, graphs and networks, applications.**

I. Introduction

Electroencephalography (EEG) is a method to measure the electrical activity of the brain using electrodes attached to the scalp at multiple locations. Synchronous electrical activity in different brain regions is generally assumed to imply functional relationships between these regions. A measure for this synchrony is EEG coherence, calculated between pairs of electrode signals as a function of frequency [1], [2].

Related studies of functional brain connectivity use other non-invasive neuroimaging techniques, including magnetoencephalography (MEG) [3]–[5] and functional magnetic resonance imaging (fMRI) [6]–[9]. A typical visualization of EEG, MEG and fMRI coherence, is a two-dimensional graph layout. Vertices represent electrodes, superconducting quantum interference devices (SQUIDS), or fMRI regions of interest (ROIs), respectively. Edges represent significant coherences between electrode signals, SQUID signals, or fMRI-ROI time series, respectively. Vertices are commonly visualized as dots and edges as lines. For multichannel EEG (e.g., [10], [11]), MEG (e.g., [4], [5]), and fMRI (e.g., [6], [8]), this layout may suffer from a large number of overlapping edges, resulting in a cluttered visualization.

In the case of EEG, the reorganization of vertex positions [12] to reduce clutter is not appropriate, because the electrodes have meaningful positions. Other solutions reorganize edges or vary visual attributes of the edges [13], [14], but do not reduce the number of edges. Several methods divide EEG electrodes [15], [16], MEG SQUIDS [3], or fMRI voxels [9] into disjoint hypothesis-driven ROIs and study coherences within or between ROIs. Other methods set out ROIs representing EEG electrodes [10], [17], MEG SQUIDS [5], or fMRI-ROIs [6] along rows and columns, thus obtaining a square contingency table. By arranging ROIs along rows and columns of a matrix, the spatial relations are lost.

Visualization of multichannel EEG (at least 64 electrodes) is not always managed well [18]–[20]. Researchers often employ a hypothesis-driven definition of certain ROIs in which all electrodes are assumed to record similar signals because of volume conduction effects [21]. As an alternative for the hypothesis-driven approach, we previously presented two methods for the detection of data-driven ROIs, referred to as functional units (FUs) [20]. An FU is represented in the coherence graph by a spatially connected clique. A clique is a vertex set in which every two-element subset is connected by an edge. A clique C is *maximal* when it is not contained in any larger clique ('larger' meaning having more vertices). Within one FU, each pair of vertices represents two significantly coherent electrode signals. In any group of vertices other than a clique, there are two vertices representing two electrode signals which are not significantly coherent. Because larger ROIs are assumed to correspond to stronger source signals, larger FUs are considered to be more interesting. Therefore, we focus on maximal cliques, for which vertex sets are as large as possible.

Our first FU detection method is a maximal clique based (MCB) method [20]. The second method is a watershed based (WB) method that detects spatially connected cliques in a greedy way [22]. However, it suffers from potential over-segmentation problems. Extending our earlier work, one of the novelties which we present is an improved watershed based (IWB) method for FU detection. It merges FUs if they are spatially connected and if their union is a clique, thus reducing over-segmentation obtained with the WB method.

In addition to individual dataset analysis, we introduce two new group maps for data-driven group analysis of multichannel EEG

Manuscript received month xx, 200x; revised month xx, 200x.

The authors are with: (a) Institute for Mathematics and Computing Science, University of Groningen, P.O. Box 800, 9700 AV Groningen, The Netherlands; (b) BCN Neuroimaging Center, University of Groningen, The Netherlands; (c) Department of Neurology, University Medical Center Groningen, University of Groningen, The Netherlands. E-mail: {mtc@cs.rug.nl, n.m.maurits@neuro.umcg.nl, j.b.t.m.roerdink@rug.nl}.

coherence as extensions of the IWB method. They serve as a data-driven alternative for the common hypothesis-driven selection of coherences for group analysis [2], [16], [23]. First, the group mean coherence map preserves dominant features from a collection of individual FU maps. Second, the group FU size map visualizes the average FU size per electrode across a collection of individual FU maps. Results are reported for an extensive case study.

II. EEG Coherence

EEG can be recorded using currently up to 512 electrodes, labeled uniquely by a combination of letters and digits (e.g., F3, Cz, P4, as in Fig. 1, right). A conductive gel is applied between skin and electrodes to reduce impedance. The electrical potential is measured at all electrodes simultaneously. The measured signals are amplified, resulting in one recording channel for every electrode. If there are many electrodes, the term 'multichannel' or 'high-density' EEG is used. As a result of volume conduction [21], multiple electrodes can record a signal from a single source in the brain. Therefore, nearby electrodes usually record similar signals. Because sources of activity at different locations may be synchronous, electrodes far apart can also record similar signals. A measure for this synchrony is coherence, calculated between pairs of signals as a function of frequency. The coherence c_λ as a function of frequency λ for two continuous time signals x and y is defined as the absolute square of the cross-spectrum f_{xy} normalized by the autospectra f_{xx} and f_{yy} [1], having values in the interval $[0,1]$: $c_\lambda(x,y) = \frac{|f_{xy}(\lambda)|^2}{f_{xx}(\lambda) f_{yy}(\lambda)}$. The cross-spectrum and auto-spectrum can be interpreted as covariance and variance as a function of frequency, respectively. An event-related potential (ERP) is an EEG recording of the brain response to a sensory stimulus. To calculate the coherence for an event-related potential (ERP) with L repetitive stimuli, the EEG data can be segmented into L segments, each containing one brain response. A significance threshold ϕ for the estimated coherence is then given by [1]

$$\phi = 1 - p^{1/(L-1)}, \tag{1}$$

where p is a probability value associated with a confidence level α ($p = 1 - \alpha$). For an overview of other common linear (and nonlinear) measures of synchrony, see [24].

III. Related Work

We discuss visualizations of functional brain connectivity obtained using the noninvasive neuroimaging techniques EEG, MEG, and fMRI. MEG commonly uses up to 512 SQUIDs to measure magnetic fields induced by electrical brain activity. Similar to EEG coherence, MEG coherence is calculated between pairs of SQUID signals. fMRI measures time series of changes in cerebral blood oxygenation levels in the brain. Often, fMRI researchers compute coherence (or other similarity) values between mean time series for different ROIs which are commonly single voxels or connected sets of voxels [7].

Although a comparison of different neuroimaging methods should be made carefully [25], the common underlying data representation for the different types of connectivity is a graph. Therefore, we restrict ourselves to graph visualizations and focus on hypothesis-driven and data-driven aspects. First, we consider EEG and MEG with typically up to 512 vertices, whose spatial relations can be represented by a planar graph. Later, we consider fMRI with vertices commonly representing thousands of voxels [7]. The overview also includes general graph drawing solutions.

A. EEG and MEG

EEG and MEG coherence graphs have vertices representing electrodes and SQUIDS, respectively. Most of the visualizations of EEG are applicable to MEG, and vice versa. For a two-dimensional visualization of the vertices, often planar projections are used of the three-dimensional electrode or SQUID locations on the surface of a head. Vertices are usually mapped to a top view of a head (e.g., Fig. 1, right), sometimes to two separate side views of the left and right hemisphere [11], [15]. Visualizations with edges representing significant coherences may suffer from a large number of overlapping edges, resulting in a cluttered visualization for multichannel EEG (e.g., [10], [11]; Fig. 1, left) or MEG (e.g., [4], [5], [26]). Existing solutions for the reduction of clutter involve an adapted visualization of the vertices and the edges.

The layout of the vertices can be changed, e.g., by using a force-directed placement [12]. However, for EEG applications we prefer to maintain the spatial relationship between the vertices representing electrodes, because electrodes have meaningful positions. A different method uses an area dependent visualization of vertices of variable size [27], but also does not preserve vertex positions. Other solutions vary (combinations of) visual attributes of vertices and edges, e.g., transparency [13], color [4]–[6], [8], saturation [14], line width [9], [14], and line style [9]. Nevertheless, the presence of many overlapping edges may still obscure other visualization elements, or the superposition of differently colored lines might result in an undesired mix of colors. Also the layout of the edges can be manipulated, e.g., by interactively curving away edges from the focus of attention [13]. This has the undesirable side-effect that, in an already crowded field of view, the area which is out of focus will be even more crowded. Moreover, to get a complete overview of the graph, every vertex (out of up to 512 vertices for EEG coherence) has to be selected individually. Alternatively, elements (such as edges) can be left out selectively [28]. Nevertheless, cluttered visualizations are even obtained for restrictions to the top 5 % coherences for only 66 MEG SQUIDS [4], or the top 10 % for 119 EEG electrodes (Fig. 1, left).

The main disadvantage of many existing analyses of multichannel EEG or MEG is the hypothesis-driven selection of the number of ROIs and the positions of the ROIs, instead of a data-driven selection. One method chooses a regularly distributed subset of electrodes [2], ignoring the majority of the electrode signals. An MEG method divides channels into disjoint hypothesis-driven ROIs and maps the average coherence within a ROI to a color [3], ignoring coherences between ROIs. A similar EEG method divides electrodes into four disjoint ROIs and studies anterior-posterior connections between those ROIs [15]. Another EEG method divides (the majority of the available) electrodes into disjoint hypothesis-driven ROIs and studies coherences between these ROIs across datasets [16], but it does not simultaneously visualize which electrodes are part of which ROI.

An existing EEG approach which is data-driven sets out up to 21 electrodes along both the rows and columns of a matrix as a tiled display [10], [17]. The result is a square contingency table showing coherence values for all possible electrode pairs. Each table entry is a square in which coherence is displayed

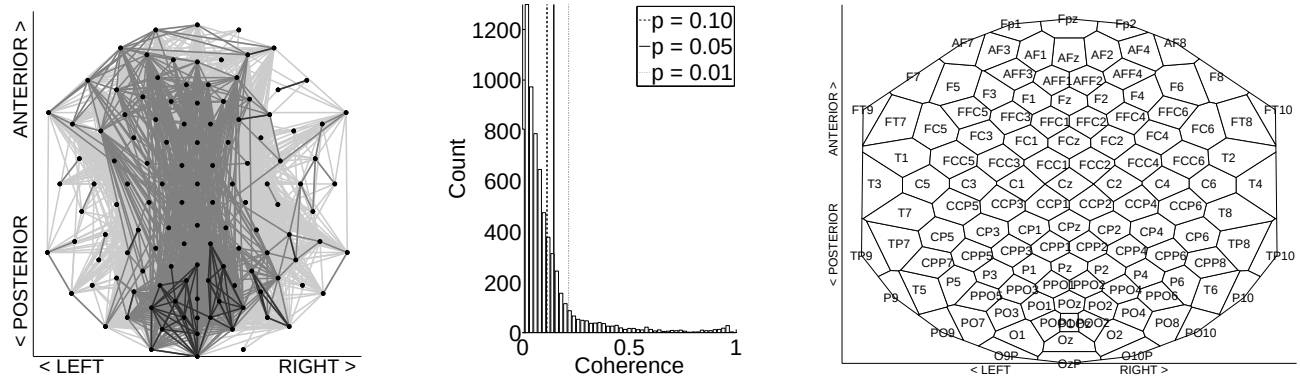

Fig. 1. **Left:** Layout of a coherence graph (EEG frequency band 1-3 Hz). Vertices represent electrodes, edges represent significant coherences between electrode signals, where the significance threshold equals 0.22 (corresponding to $p = 0.01$). Edges are visualized as gray lines, vertices as black dots. An edge is light gray if its value is in the range $0.22 < c_\lambda < 0.37$, medium gray if its value is in the top 10 % of the coherences ($0.37 \leq c_\lambda < 0.91$), and dark gray if its value is in the top 1 % ($c_\lambda \geq 0.91$). This corresponds to a common existing data-driven visualization, showing cluttered edges. **Middle:** Histogram of the corresponding coherences to illustrate the coherence distribution. Vertical lines (dash, solid, dot) indicate significance thresholds associated with three probability levels ($p = 0.10, 0.05, 0.01$, respectively). **Right:** Voronoi diagram with electrode labels in the corresponding cells. The convex hull of all electrodes is shown as a boundary. To improve the readability, the Voronoi diagram is stretched horizontally. Because the coherence computation is independent of distance, distances between electrodes do not need to be preserved. However, spatial relationships between electrodes are maintained.

between the two corresponding electrode signals as a function of frequency. By arranging the electrodes along the rows and the columns of the matrix, the spatial relations are lost. As a result, consecutive entries in the table do not need to imply coherence between pairs of signals recorded at adjacent electrodes on the scalp. Similarly, a square contingency table is created for 78 MEG SQUIDS sorted into four hypothesis-driven ROIs [5] (left/right, anterior/posterior). Each table entry is square with the coherence of the corresponding signals mapped to a color. A different data-driven EEG approach first localizes dipoles corresponding to maximally independent components in the data, and then calculates and visualizes coherence between dipole activities [29]–[31]. However, dipole source solutions are not unique [32].

Another approach is restricted to local EEG coherence, which is defined as the coherence between two spatially neighboring electrodes [33], [34]. It requires additional methods to study coherences between electrodes which are not direct spatial neighbors. Another visualization creates a map of topographic submaps [35], with one submap for each electrode visualizing the coherence between itself and every other electrode. It does not explicitly visualize coherence between electrodes by connecting lines. As a consequence, every topographic submap (out of up to 512 submaps) needs to be studied separately to obtain a complete overview. Another drawback is that local coherences dominate the visualization [35]. A subselection of two topographic submaps out of 128 is made in [23], without providing a complete overview of all coherences.

B. fMRI

For fMRI coherence, usually a limited number of so-called seed (or reference) voxels is selected on the basis of prior anatomical or functional information. However, the anatomy may be abnormal, and the choice of seed points may affect the results [7]. Nonetheless, either an individual seed point or a spatially connected set of voxels including a seed point is considered as a ROI having a (mean) time series. Vertices represent ROIs and can be visualized three-dimensionally [36] or two-dimensionally. A two-dimensional visualization uses, e.g., a planar projection of three-dimensional ROI positions or an approximation of functional distances by graphical distances using metric multidimensional scaling [9]. An edge represents a significant similarity between two ROI time series. The visualization of edges as lines may lead to clutter [6], [8], [9], [36].

Filtering edges may still lead to cluttered visualizations [6]. Other visualizations set out ROIs along the rows and columns, thus obtaining a square contingency table. Each table entry is a square with a similarity value between the two corresponding signals mapped to a color [5], [6]. Existing data-driven graph clustering algorithms include hierarchical cluster analysis [7] and independent component analysis (ICA) [29], [30], [37]. The result of hierarchical cluster analysis can be visualized as a dendrogram [9], showing the ROIs as leaves of a binary tree, thus losing the spatial relations between the ROIs. Also, ROIs can be visualized as colored volumes of interest [37] which may occlude each other. For the same reason, we do not favor three-dimensional EEG visualizations. Alternatively, ROIs can be visualized on anatomical slices [7], [9], [38]. However, a large number of two-dimensional slices is required to obtain a complete overview of a three-dimensional volume. Sometimes, instead of an explicit visualization of the connection between ROIs (e.g., with a line), all ROIs in one cluster are colored identically, with different colors and/or separate slices for different clusters [9].

C. Conclusion

The overview of related work has concentrated on the requirements we posed on an EEG coherence visualization: it should be (1) data-driven, (2) preserve electrode locations, (3) minimize visual clutter, and (4) present an overview. Many of the discussed methods still suffer from visual clutter or relocate vertices and edges and therefore do not meet requirement (2) or (3). On the other hand, existing methods which do meet requirements (2,3) are hypothesis-driven, thus failing to meet our requirement (1). In summary, the method proposed in this paper combines a number of features which no single technique currently provides.

IV. Data Representation

A. Experimental Setup

Brain responses from two groups of five younger (34 ± 10 years, mean $\pm$ standard deviation) and five older (62 ± 8 years) adults are studied, which were recorded using an EEG cap with 119 scalp electrodes. During a so-called P300 experiment, each participant was instructed to count target tones of 2000 Hz (probability 0.15), alternated with standard tones of 1000 Hz (probability 0.85) which were to be ignored. After the experiment, the participant had to report the number of perceived target tones. For each dataset, brain responses to 20 target tones were recorded in $L = 20$ segments of 1 s. EEG coherence is influenced by the choice of reference. We chose to use an average reference, which is a close-to-optimal approximation to a reference-free recording in the case of 128 electrodes [2], [39].

A procedure from *Neurospec* was adopted to compute the coherence (`www.neurospec.org`). We first averaged over segments and then over adjacent spectral lines in predefined frequency bands. Frequencies between 1 and 30 Hz are typically studied clinically. We calculated the average coherence within five EEG frequency bands (1-3, 4-7, 8-12, 13-20, and 21-30 Hz), because EEG synchrony varies with frequency [2], [39]. For 119 electrodes, in total 7021 coherence values were computed per frequency band. If the conductive gel accidentally connected two adjacent electrodes, very high coherences were measured. Coherences higher than 0.99 were therefore ignored. Typically, this threshold value eliminates approximately 0.01% of the coherences. Note also that using Eqn. 1 for determining significance levels is a coarse approximation, since it does not take the number of spectral lines per band into account. However, this approximation only overestimates the significance level, and does not influence the visualization method itself.

B. EEG Coherence Graph

The data are represented by an undirected *coherence graph* with vertices representing electrodes. Coherences above the significance threshold (Eqn. 1) are represented by edges, coherences below the threshold are ignored. Vertices are not self-connected. To determine spatial relationships between electrodes, a Voronoi diagram is employed which partitions the plane into regions of points with the same nearest vertex. For EEG data, the vertex set equals the set of electrode positions (Fig. 1, right). The vertices are referred to as (Voronoi) centers, the region boundaries as (Voronoi) polygons. The area enclosed by a polygon is called a (Voronoi) cell. We call two cells *Voronoi neighbors* if they have a boundary in common. A collection of cells C is called *Voronoi-connected* if for a pair $\phi_0, \phi_n \in C$ there is a sequence $\phi_0, \phi_1, ..., \phi_n$ of cells in C with each pair ϕ_{i-1}, ϕ_i consisting of Voronoi neighbors. Cells, vertices, and electrodes are interchangeable for the use with the terms 'Voronoi neighbor' and 'Voronoi-connected'.

V. FU Detection

Whereas there are many unsupervised graph clustering methods, e.g., hierarchical clustering and ICA (see Section III), our choice is motivated by the type of cluster we desire. As a result of volume conduction [21], multiple electrodes can record a signal from a single source. Consequently, a spatially connected set of electrodes recording similar signals is considered as a data-driven ROI (a cluster). Such a ROI is referred to as functional unit (FU) and is represented in the EEG coherence graph by a clique consisting of a set of spatially connected vertices [20].

Recall that larger ROIs are assumed to correspond to stronger source signals and are considered to be more interesting. Therefore, our first method for FU detection is primarily based on the detection of maximal cliques [40], [41]. We adapted this method to detect spatially connected sets of vertices [20]. Our second method for FU detection is based on watersheds, an efficient method for detecting spatially connected segments [42]. We adapted this method to detected cliques in a greedy way [22]. Next, we first briefly describe the two earlier developed FU detection methods, before introducing a novel improved method based on watersheds which is designed to reduce over-segmentation.

A. Maximal Clique Based (MCB) Method

1) Maximal Cliques: Bron and Kerbosch (B&K) [40] developed a method to detect all maximal cliques in a graph. It first branches the problem, and bounds unsuccessful branches. Its recursive procedure maintains three dynamic vertex sets:

- the set *compsub* contains an increasing or decreasing clique;
- the set *candidates* contains vertices that are connected to all vertices in *compsub* and that can be added to *compsub*;
- the set *not* contains vertices that are connected to all vertices in *compsub* and that were added to *compsub* previously.

At each call of the procedure, the vertex v from the set *candidates* is selected that has the largest number of connections with the other vertices in *candidates*. If there are more such vertices, then one of these is randomly selected. Further, it is assured that v is not connected to the vertex just added to *not*. The selected vertex v is added to *compsub* and removed from *candidates*. Next, *newcandidates* is the intersection of *candidates* and the neighborhood of v. Similarly, *newnot* is the intersection of *not* and the neighborhood of v. If both *newcandidates* and *newnot* are empty, *compsub* is a maximal clique. This procedure is repeated recursively with local sets *newcandidates* and *newnot*, until the candidate set is empty. In case the procedure is not repeated with *newcandidates* and *newnot*, the vertex most recently added to *compsub* (vertex v) is removed from *compsub* and added to *not*. If any vertex in *newnot* is connected to all vertices in *newcandidates*, then it is known that this vertex will never be removed from *not* and this branch is bounded.

The worst-case time complexity for detecting all maximal cliques is $O(3^{n/3})$, with n the number of vertices, because $3^{n/3}$ is the highest number of cliques [41]. In practice, performance of maximal clique detection strongly depends on graph structure [43].

2) Voronoi-Connected Maximal Cliques: We extended the method [40] such that it only detects maximal cliques consisting of Voronoi-connected vertices [20]. The three dynamic vertex sets are maintained, but the set *candidates* is split into a set *currentcand* and a set *complcand*. The set *currentcand* contains the candidates that are Voronoi neighbor of at least one element in *compsub*; only these can be added to *compsub* at the current step. The set *complcand* is the complement of *currentcand* in *candidates*. At each call, the element from *currentcand* which has the largest number of connections with the other candidates (*currentcand* $\cup$ *complcand*) is added to *compsub*. Let this element be v'. The set *newcurrentcand* is the intersection of *currentcand*

and the neighborhood of v' (in the coherence graph), united with the Voronoi-neighbors of v' in *complcand*. The set *newcomplcand* is the intersection of *complcand* and the neighborhood of v' (in the coherence graph), minus the Voronoi-neighbors of v' in *complcand*. The set *(new)not* is maintained as before. This is repeated until *newcurrentcand* is empty. If *newnot* is also empty, then *compsub* is a Voronoi-connected maximal clique.

Fig. 2 illustrates maximal clique detection with the B&K algorithm (A and B) and Voronoi-connected maximal clique detection with the MCB method (C), for a graph with the adjacency matrix shown in Table I. The first B&K iteration has an empty *not* set (A). One of the later recursive iterations of the B&K method returns to the initial situation with all vertices in the *candidates* set (not shown), puts the selected vertex labeled c in the not set (B1), and selects the vertex with the highest degree in the *candidates* set (B2). Whereas the B&K method detects maximal cliques which can consist of more than one spatial component (A5), the MCB method detects spatially connected cliques instead (C4). (For the MCB method, the use of the *not* set is the same as for the B&K method and is therefore not explicitly illustrated.)

The following detailed description contains (row, column) references to Fig. 2. **C5.** Vertex positions. Vertices are spatial neighbors if they are 4-connected (e.g., the spatial neighbors of vertex d are vertices a, e, and g). **A.** Iteration of B&K maximal clique detection with empty *not* set. It starts with all nine vertices in the set candidates (not illustrated). **A1.** Then the vertex c with the highest degree (following Table I) is first added to *compsub*; its adjacent vertices are in *candidates*. (Vertices not part of any set are shown as a black dot.) **A2-A4.** At every next step, the vertex with the highest degree in *candidates*, let us say v, is added to *compsub*. (In the case of ties one vertex is selected randomly.) Further, vertices not adjacent to v (denoted by $\Gamma^c(v)$) are removed from *candidates*. This continues until *candidates* is empty. At **A2**, $v = b$, $\Gamma^c(v) = \{d\}$; at **A3**, $v = g$, $\Gamma^c(v) = \{e\}$; at **A4**, $v = f$, $\Gamma^c(v) = \{h\}$; at **A5**, $v = i$, $\Gamma^c(v) = \emptyset$. Now, *compsub*= $\{b, c, f, g, i\}$ is a maximal clique, because *candidates*= $\emptyset$ (and *not*= $\emptyset$). **B.** A later iteration for B&K maximal clique detection returns to the situation preceding A1 with all vertices in the candidates set, and puts the first selected vertex c into the *not* set. **B1.** Vertex c which was previously selected first (see A1) is now in the *not* set. **B2-B4.** Similar to A2-A4. **B5.** Different from A5, now *candidates* = $\{b, f, g, i\}$, and *not* = $\{c\}$. This implies that the maximal clique $\{b, c, f, g, i\}$ has been found before. **C.** MCB Voronoi-connected maximal clique detection with same starting point as A (with *not* = $\emptyset$). **C1.** The vertex c with the highest degree is first added to *compsub*; its adjacent vertices (see Table I) are in *currentcand* if they are a spatial neighbor ($\{b, f\}$), or otherwise in *complcand*. **C2-C4.** At every next step, the element from *currentcand* which has the largest number of connections with the other candidates (*currentcand* $\cup$ *complcand*) is added to *compsub*. The spatial neighbors of v' in *complcand* (denoted by $\Lambda(v')$) are moved from *complcand* to *currentcand*. Further, vertices not adjacent to v' (i.e., $\Gamma^c(v')$) are removed from both *currentcand* and *complcand*. This continues until *currentcand* is empty. At **C2**, $v' = b$, $\Lambda(v') = \{e\}$, $\Gamma^c(v') = \{d\}$; at **C3**, $v' = f$, $\Lambda(v') = \{i\}$, $\Gamma^c(v') = \{h\}$; at **C4**, $v' = i$, $\Lambda(v') = \emptyset$, $\Gamma^c(v') = \{e\}$. **C4.** *compsub*= $\{b, c, f, i\}$ is a spatially connected maximal clique, because *currentcand* = $\emptyset$ (and *not* = $\emptyset$). Remaining vertices in *complcand* are in the adjacency list of all vertices in *compsub* but are not a spatial neighbor of any vertex in *compsub*.

TABLE I

ADJACENCY MATRIX FOR VERTICES a THROUGH i IN FIG. 2 (1 (0) MEANS (NOT) CONNECTED).

	a	b	c	d	e	f	g	h	i
a	0	0	0	1	0	0	0	0	0
b	0	0	1	0	1	1	1	1	1
c	0	1	0	1	1	1	1	1	1
d	1	0	1	0	0	0	0	0	0
e	0	1	1	0	0	1	0	0	0
f	0	1	1	0	1	0	1	0	1
g	0	1	1	0	0	1	0	1	1
h	0	1	1	0	0	0	1	0	0
i	0	1	1	0	0	1	1	0	0

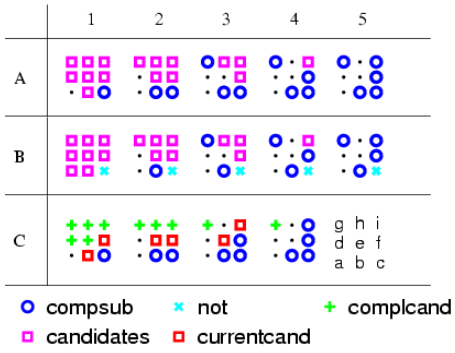

Fig. 2. Illustration of maximal clique detection with the B&K algorithm for an iteration with an empty *not* set (**A**) and an iteration with a non-empty *not* set (**B**), and Voronoi-connected maximal clique detection with the MCB method (**C**), for a graph with adjacency matrix as in Table I. For explanation, see text.

3) FU Labeling: Every vertex can be part of multiple (Voronoi-connected) maximal cliques. To assign a unique label to every vertex, a quantity *total strength* is defined for a (sub)graph $G = (V, E)$ as the sum of all edge values [20]. This value is not normalized for the size of E. Consequently, if two graphs have an equal average coherence, the graph with more vertices has a higher total strength. Next, all cliques are queued in decreasing order by their total strength. Then the following labeling procedure is repeated, until there are no more cliques or until all vertices are labeled. The first clique is removed from the queue, and all its vertices are assigned a unique label and are removed from the other cliques. If necessary, the changed cliques are separated into Voronoi-connected components. For all changed cliques, the total strength is recomputed before they are put in the appropriate position in the sorted queue. After completion of the labeling procedure, every set of identically labeled vertices is an FU.

B. Watershed Based (WB) Method

The watershed based (WB) method is an alternative to the standard MCB method [22]. It is a greedy method approximating spatially connected maximal cliques on the basis of an edge-based watershed transform. The WB method defines as markers those vertices which are locally maximally similar to their spatially neighboring vertices. To obtain the markers, a coherence value is assigned to each vertex by computing the average of the edge values between this vertex and all its Voronoi neighbors. Then, all vertices which are local maxima are considered as markers to be associated with basins. (A similar edge-based watershed method,

which is not restricted to detect cliques, instead selects pairs of vertices as markers which are incident with an edge which is a local minimum [44].)

The WB method for greedy Voronoi-connected clique detection maintains the following dynamic vertex sets.

- *bsn*$_i$ contains a sorted list of the vertices in basin i.
- $L(v)$ contains the basin label of vertex v.
- *adjCBsn*$_i$ contains a list of vertices (sorted by vertex number) which are adjacent to *each* of the vertices in *bsn*$_i$ in the coherence graph.
- *queue* contains edges in decreasing order. When vertex v receives a label, an edge $e = (v, v')$ is added to *queue* for each unlabeled Voronoi neighbor v' of v, provided that the corresponding edge value exceeds the significance threshold (Eqn. 1).

Whereas the usual queue-based implementation of the watershed transform applied to digital images uses a *vertex* queue sorted in increasing order of value [45], we use an *edge* queue sorted in decreasing order of coherence value. (The vertex values are only used for defining the markers.) In case the coherence graph has multiple identical edge values (which did not occur for our datasets), an ordered queue consisting of queues with identically valued elements can be used [45]. We now turn to a more precise analysis of the algorithm.

(Step 1) The edge queue is initialized with edges (corresponding with a significant coherence) between markers and their Voronoi neighbors. The first edge (v, v') in this queue corresponds to the highest similarity (coherence) between any vertex v' outside and a Voronoi neighboring vertex v inside a basin. Therefore, vertex v' is the first candidate to be added to a basin.

(Step 2) The main procedure consists of the following steps. Remove the first edge, say $e = (v, v')$ from *queue*. In case vertex v' was also labeled between the insertion and removal of $e = (v, v')$, nothing is done and the procedure continues with a new edge. Otherwise (v' is unlabeled), there are two cases. (i) In case $v' \in$ *adjCohBsn*$_{L(v)}$ (line 20), v' receives label $L(v)$ and (ii) *adjCohBsn*$_{L(v)}$ is replaced by its intersection with the neighborhood of v' in the coherence graph (line 22); (iii) v' is added to *bsn*$_{L(v)}$ (line 23); (iv) *queue* is extended with the edges between v' and its Voronoi-neighbors (line 24-28), provided that corresponding edge values exceed the significance threshold. In the other case, if $v' \notin$ *adjCohBsn*$_{L(v)}$, v' is not labeled (yet). This procedure is repeated until *queue* is empty. Each basin then corresponds to an FU.

The time complexity of the WB method is $O(n^2 \log n)$, with n the number of vertices [22].

C. Improved Watershed Based (IWB) Method

Over-segmentation is a potential problem of the WB method. To reduce over-segmentation we here implement the first solution suggested in [22], by merging two spatially neighboring FUs if their union is a clique in the coherence graph. To obtain the improved watershed based (IWB) algorithm (Alg. 1) we insert lines 12-16 and lines 30-43 in the pseudocode of the WB algorithm (see also [22]). In words, the difference between the WB and IWB method is the following. In case vertex v' was labeled between the insertion and removal of $e = (v, v')$, nothing is done if the label of v' is equal to the label of v. Otherwise ($L(v') \neq L(v)$), see line 30), the following steps are executed consecutively (for notation purposes, define ψ as $L(v')$): (i) check if all vertices in *bsn*$_{L(v)}$ are in *adjCohBsn*$_\psi$, and vice versa (line 33). (ii) Replace *bsn*$_{L(v)}$ by the union of itself with *bsn*$_\psi$, because their union is a spatially connected clique in the coherence graph (line 34); (iii) all vertices in *bsn*$_\psi$ receive the label $L(v)$ (lines 35-37); (iv) *adjCohBsn*$_{L(v)}$ is replaced by the intersection of itself with *adjCohBsn*$_\psi$ (line 38); (v) *bsn*$_\psi$ and *adjCohBsn*$_\psi$ are made empty (line 39).

In the algorithm, the operation *insertEdgeSort(e*(v, v')*,queue)* inserts edge *e*(v, v') into the appropriate position in a edge queue *queue* which is decreasingly sorted by edge value; similarly, *insertVSort(v,vqueue)* inserts vertex v into the appropriate position in vertex queue *vqueue* which is decreasingly sorted by vertex number; *dequeue(queue)* returns and removes the first edge from an edge queue *queue*; *intersect(.,.)* gives the intersection of two sorted vertex sets; *merge(.,.)* gives the union of two sorted vertex sets (without duplicates); *setInSet(*V*,*V'*)* returns 'true' if the sorted vertex set V is a subset of the sorted vertex set V', and 'false' if not. The size of a vertex set is denoted by $|\ .\ |$.

One adaptation further improves the average performance in practice. A matrix *bsnMat* is created with the basins set out along the rows and the columns, and is initialized with only ones (lines 12-16). If two spatially neighboring basins b_i and b_j together are not a clique, then *bsnMat*(b_i, b_j) and *bsnMat*(b_j, b_i) are set to zero (line 41). In that case, basins b_i and b_j cannot be merged later either, and lines 32-42 are skipped the next time that b_i and b_j are candidates to be merged.

The difference between the WB and the IWB method affects the time complexity as follows. (i) line 33: the check to see if one sorted list is part of another has time complexity $O(n)$. Each of the next steps also has time complexity $O(n)$ for sorted lists of vertices of at most length n: (ii) line 34: taking the union of two sorted lists, (iii) lines 35-37: labeling a list, (iv) line 38: intersecting two sorted lists, (v) line 39: making lists empty. Steps (i)-(v) are executed $O(n)$ times (recall that the order of the number of edges between Voronoi neighbors in *queue* is $O(n)$). Thus, the time complexity of the IWB adaptation is $O(n^2)$ and the time complexity for the complete IWB algorithm is the same as for the WB method, i.e., $O(n^2 \log n)$.

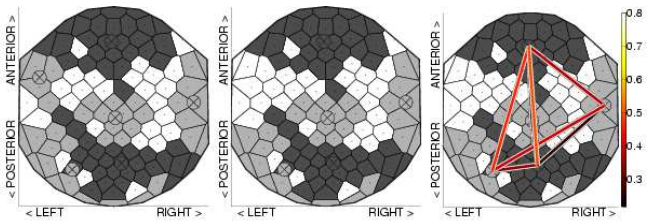

Fig. 3. IWB FU map (EEG frequency band 1-3 Hz, dataset young 5). Top view, nose on top. **Left:** A circle with a cross inside indicates the geographic center of all Voronoi centers belonging to one FU. **Middle:** The same FU map, but only with FUs larger than 5 cells. White Voronoi cells are part of smaller FUs. **Right:** Lines connect FU centers if the inter-FU coherence exceeds the significance threshold (Eqn. 1). The color of the line depends on the inter-FU coherence (see color bar, with minimum corresponding to the coherence threshold $\phi \approx 0.22$ for $p = .01$).

VI. FU Visualization

A. FU Map for Individual Dataset Analysis

Given the FUs, the *inter-FU coherence* c'_λ at frequency λ between two FUs W_1 and W_2 is defined as the sum of the

Algorithm 1 IWB pseudocode. Lines 12-16 and 30-43 were inserted into the WB method to obtain the IWB method.

INPUT: V is the vertex set; *marker(i)* = marker *i*;
$c(v, v')$ = coherence(v, v') = $c(v', v)$;
adjCoh$_v$ = $\{v' \in V \mid c(v,v') \geq \phi\}$; ϕ = *sign. threshold*
adjVor$_v$ = $\{v' \in V \mid v' \in$ Vor.-neighbors$_v$ & $v' \in$ adjCoh$_v\}$;
{*adjCoh*$_v$, *adjVor*$_v$ are both sorted by vertex number}
OUTPUT: *bsn*$_i$ is basin i (i.e., an FU) sorted by vertex number
INITIALIZATION:
1: queue $\leftarrow \emptyset$ {queue of edges}
2: **for all** $v \in V$ **do**
3: $L(v) \leftarrow 0$ {$L(v)$ = label of vertex v}
4: **end for**
5: **for** $i = 1$ to |marker| **do**
6: bsn$_i \leftarrow$ marker(i); $v \leftarrow$ marker(i); $L(v) \leftarrow i$
7: adjCBsn$_{L(v)} \leftarrow$ adjCoh$_v$
8: **for all** $v' \in$ adjVor$_v$ **do**
9: insertEdgeSort(e(v,v'),queue)
10: **end for**
11: **end for**
12: **for** $i = 1$ to |marker| **do**
13: **for** $j = 1$ to |marker| **do**
14: bsnMat$(i, j) \leftarrow 1$ {IWB modification}
15: **end for**
16: **end for**
MAIN:
17: **while** queue $\neq \emptyset$ **do**
18: e$(v, v') \leftarrow$ dequeue(queue)
19: **if** $L(v')$ = 0 **then**
20: **if** $v' \in$ adjCBsn$_{L(v)}$ **then**
21: $L(v') \leftarrow L(v)$
22: adjCBsn$_{L(v)} \leftarrow$intersect(adjCBsn$_{L(v)}$,adjCoh$_{v'}$)
23: bsn$_{L(v)} \leftarrow$ insertVSort(v',bsn$_{L(v)}$)
24: **for all** $v^* \in$ adjVor$_{v'}$ **do**
25: **if** $L(v^*) = 0$ **then**
26: insertEdgeSort(e(v', v^*),queue)
27: **end if**
28: **end for**
29: **end if**
BEGIN IWB
30: **else**
31: **if** $(L(v') \neq L(v))$ **and** (bsnMat$(L(v'), L(v)) \neq 0$) **then**
32: $\psi \leftarrow L(v')$
33: **if** setInSet(bsn$_{L(v)}$,adjCBsn$_\psi$) **and** setInSet(bsn$_\psi$,adjCBsn$_{L(v)}$) **then**
34: bsn$_{L(v)} \leftarrow$ merge(bsn$_{L(v)}$,bsn$_\psi$)
35: **for all** $w' \in$ bsn$_\psi$ **do**
36: $L(w') \leftarrow L(v)$
37: **end for**
38: adjCBsn$_{L(v)} \leftarrow$ intersect(adjCBsn$_{L(v)}$,adjCBsn$_\psi$)
39: bsn$_\psi = \emptyset$; adjCBsn$_\psi = \emptyset$
40: **else**
41: bsnMat$(L(v), \psi) \leftarrow 0$; bsnMat$(\psi, L(v)) \leftarrow 0$
42: **end if**
43: **end if**
END IWB
44: **end if**
45: **end while**

coherence values between one vertex in W_1 and the other vertex in W_2, scaled by the maximal number of edges between W_1 and W_2 [20]:

$$c'_\lambda(W_1, W_2) = \frac{\sum_{i,j}\{c_\lambda(v_i, v_j) \mid v_i \in W_1, v_j \in W_2\}}{|W_1| \cdot |W_2|}. \quad (2)$$

Note that coherences between *any* pair of vertices are taken into account to normalize for the size of the FUs.

An FU map visualizes each FU as a set of Voronoi cells with identical gray value, with different gray values for adjacent FUs [20], see Fig. 3. Note that the geographic center of an FU can be located in a cell not belonging to the corresponding FU. A line is drawn between FU centers if the corresponding inter-FU coherence exceeds a threshold (Fig. 3, right). We consistently choose this threshold to be equal to the significance threshold (Eqn. 1), as we already used this threshold to determine the coherence graph.

Because larger FUs are considered to be more interesting, only FUs larger than 5 cells are considered. White Voronoi cells are part of smaller FUs.

B. Data-Driven Group Analysis

FU maps differ from individual to individual, making group analysis difficult. Therefore, we present a data-driven method for group coherence analysis which detects common features in a collection of individual FU maps. Group coherence analyses are commonly based on group means of coherences of interest. We show how our data-driven ROIs, i.e., the FUs, lead to a data-driven selection of coherences of interest.

1) Group Mean Coherence Map: We define a group mean coherence graph as the graph containing the mean coherence for every electrode pair computed across a group. To obtain a data-driven coherence visualization for a group, the group mean coherence graph is thresholded, maintaining only the edges with a value exceeding the coherence threshold (Eqn. 1). Next, an FU map is created for the group mean coherence graph, referred to as *group mean coherence map*.

2) Group FU Size Map: A group FU size map visualizes the average FU size for every electrode across a group, based on the FU maps for every individual dataset. The average FU size s of an electrode v is computed as

$$s(v) = \sum_{\text{all datasets}} \frac{\{|W| \mid v \in W\}}{\#\text{datasets}}. \quad (3)$$

with W the FU containing v in every FU map. The value s for an electrode is mapped to the gray value of its corresponding Voronoi cell, with lighter gray for higher average FU sizes, similar to a (gray scale) topographic map [19]. Consequently, a light Voronoi cell indicates that the corresponding electrode is on average part of large FUs.

VII. RESULTS

Throughout this section, we use $p = 0.01$. The corresponding coherence threshold is $\phi \approx 0.22$ (Eqn. 1).

A. FU Map

For a comparison of FU maps obtained with the three different FU detection methods, see Fig. 4. FU maps for the five datasets in each group and each of the five frequency bands are shown in Fig. 5 to 8 for the MCB and IWB method.

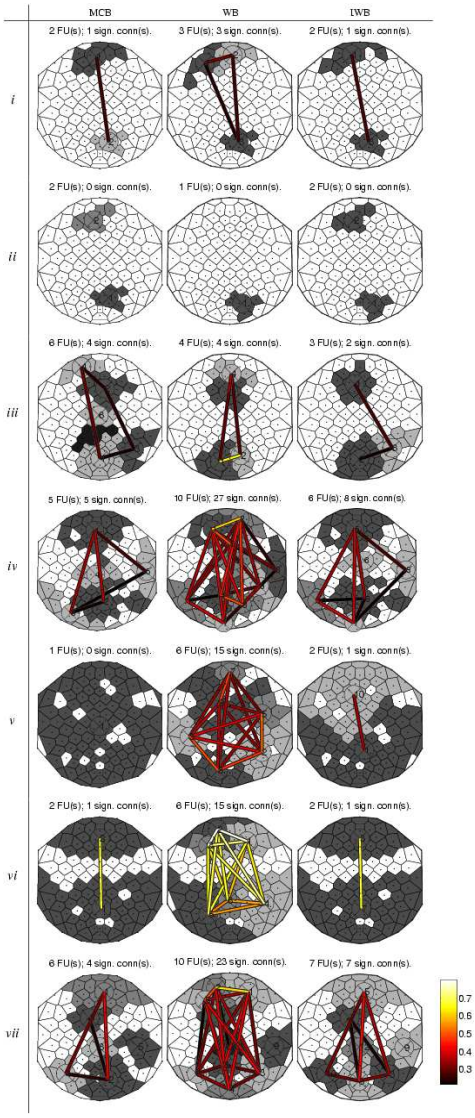

Fig. 4. Illustration of FU maps (top view, nose on top) obtained with the three FU detection methods for seven (*i-vii*) selected datasets and frequency bands. **Left:** MCB method (see also Fig. 5 and Fig. 6). **Middle:** WB method with over-segmentation. **Right:** IWB method with over-segmentation reduction (see also Fig. 7 and Fig. 8). Datasets: *(i) young 1*, 4-7 Hz; *(ii) young 1*, 8-12 Hz; *(iii) young 3*, 4-7 Hz; *(iv) young 5*, 4-7 Hz; *(v) old 2*, 1-3 Hz; *(vi) old 4*, 1-3 Hz; *(vii) old 4*, 8-12 Hz. For every dataset, the IWB FU map shows a number of FUs and a number of inter-FU connections closer to the MCB FU maps than the WB FU maps.

FU detection with the (non-optimized) MCB method was faster for smaller FU sizes, taking approximately 1 s for datasets with small FUs, up to 2 h for a dataset with the largest FU. FU detection with the (non-optimized) WB method took around 0.04 ± 0.02 s (max. 0.14 s) and with the (non-optimized) IWB method around 0.05 ± 0.04 s (max. 0.25 s). Consequently, the WB and IWB methods are up to a factor of 100,000 faster than the MCB method for this typical multichannel EEG setting with 128 channels.

Because the MCB method is assumed to obtain the most interesting FUs corresponding to the strongest source signals (Section V), it is here considered as the gold standard. We compared the WB and the IWB method with the MCB method, and made an illustrative selection of seven (out of fifty) cases (Fig. 4). The selection includes those settings (a combination of participant and frequency band) which result in the largest difference between the MCB, WB, and IWB methods. The order of the seven illustrations is chosen such that it facilitates the discussion.

i. The one anterior FU detected by the MCB method is represented by two (smaller) spatially connected anterior FUs by the WB method, whereas the IWB method merges two anterior FUs. Because the WB and IWB methods both follow a greedy approach, the anterior FUs do not correspond exactly to the anterior FU of the MCB FU map. Because the IWB method merges FUs during segmentation (and not afterwards, such as with hierarchical watersheds [44]), the vertices in the large anterior FU of the IWB FU map do not exactly correspond to the vertices that are part of the smaller anterior FUs obtained by the WB method.

ii. Although multiple anterior FUs are obtained with the WB method, they are smaller than the minimum size and therefore not shown, whereas the IWB method merges smaller FUs into an anterior FU identical to the anterior FU found with the MCB method.

iii. This is one of the occurrences of the maximal absolute difference in the number of FUs between the MCB (6 FUs) and IWB method (3 FUs). Nevertheless, the connection between an anterior and posterior region which is visible in the MCB FU map is preserved in the IWB FU map.

iv. This is one of the occurrences of the maximal absolute difference in the number of FUs between the MCB (5 FUs) and WB method (10 FUs). Whereas the WB method shows visually cluttered edges, the IWB method gives a better overview more similar to the MCB method.

v. The significance threshold used is apparently too low, as one very large FU is found with the MCB method and two very large FUs are found with the IWB method; the WB method, however, results in 6 FUs completely connected by 15 lines and does not (directly) make clear that the used threshold is too low.

vi. Both FUs found with the MCB and the IWB method are identical. The WB method has more FUs in the same region instead.

vii. The large anterior FUs found with the MCB and the IWB method are identical. The WB method has multiple FUs in the same region instead.

In all cases, the number of FUs and their size and locations are highly similar for the MCB FU maps and the corresponding IWB FU maps (Figs. 5–8). The absolute difference in the number of FUs between the WB and the MCB methods is on average 1.8 with a maximum difference of five FUs (four occurrences). The same difference between the IWB and the MCB is clearly smaller: 0.9 with a maximum of three FUs difference (two occurrences). As for the connections between FUs, those found with the MCB method are generally also found in the corresponding IWB FU maps. In particular, connections between a middle anterior and a middle posterior FU are present in the MCB FU map if and only if they are present in the corresponding IWB FU map, with one exception: for dataset *old 5*, 21-30 Hz, the inter-FU coherence is just above the threshold for the IWB method, contrary to the MCB method. For datasets *old 2* and the frequencies 1-3 Hz, the connection between anterior and posterior regions is explicit in the IWB FU map (Fig. 8) and implicit in the MCB FU map (Fig. 6: the fact that one large FU consists of nearly all vertices implies that most anterior and most posterior vertices are completely

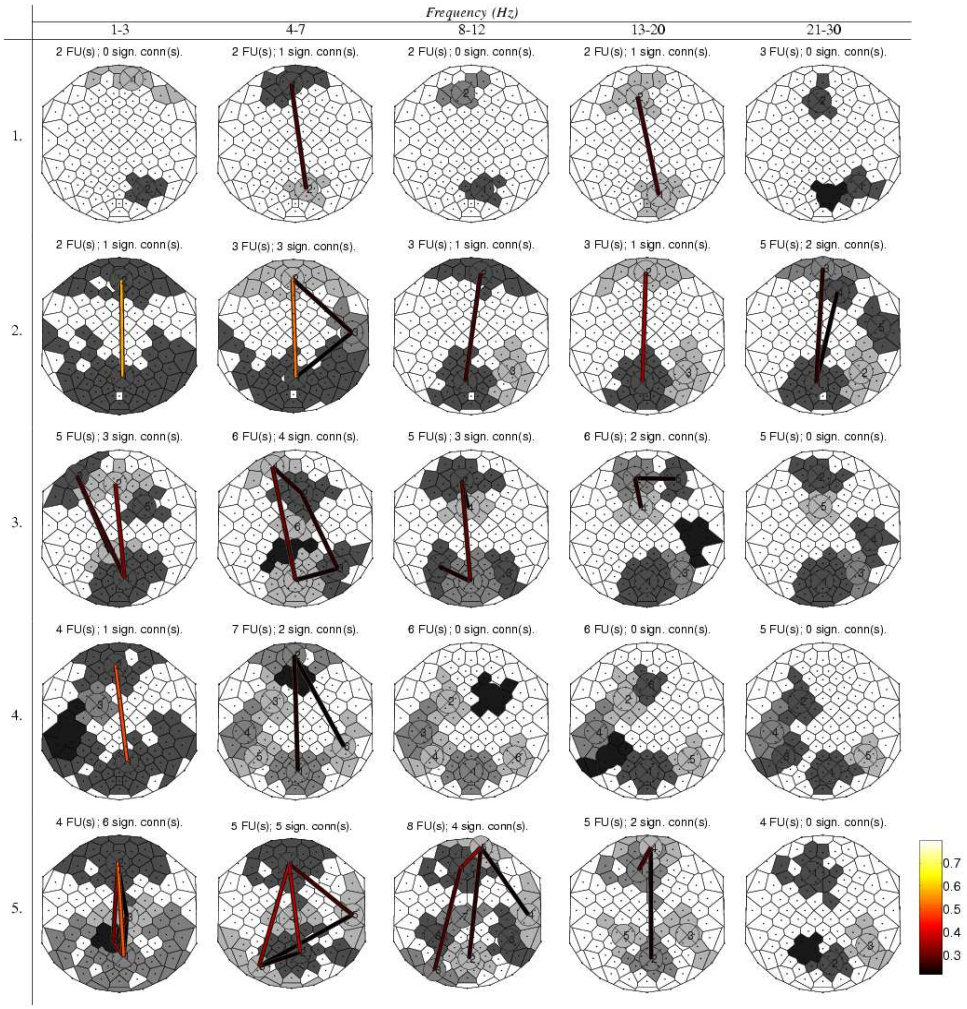

Fig. 5. **Standard MCB FU maps, younger adults**. Top view, nose on top. FU maps ($|FU| > 5$, $p = 0.01$) for five younger adults for five frequency bands (1-3, 4-7, 8-12, 13-20, 21-30 Hz). Each FU is visualized as a set of Voronoi cells with identical gray value, with different gray values for adjacent FUs. White Voronoi cells are part of FUs with $|FU| \leq 5$. A line connects FUs if the inter-FU coherence exceeds the significance threshold, with its color depending on the value (see color bar, bottom right, with minimum corresponding to the coherence threshold $\phi \approx 0.22$ for $p = 0.01$; the color bar is the same for all FU maps). Above each group mean coherence map, the number of FUs and the number of connecting lines between FUs are displayed.

connected).

B. Group Analysis

Group mean coherence maps (Fig. 9) and group FU size maps (Fig. 10) were obtained as extensions of the IWB FU detection method. They are shown for the two groups of younger and older adults and the five frequency bands.

1) Individual FU Maps versus Group Mean Coherence Maps: The largest FUs for individual datasets of younger adults (Figs. 5, 7) are mostly located anteriorly and posteriorly in the middle. This feature is also preserved in the corresponding group mean coherence maps (Fig. 9, left column). FU maps for older adults (Figs. 6, 8) usually show more lateral FUs, which are preserved in the corresponding group mean coherence maps (Fig. 9, right). For both younger and older adults, the number of FUs usually does not change much across frequency bands in the individual dataset FU maps (Figs. 5–8, compare rows), as well as in the group mean coherence maps (Fig. 9, compare rows). In four out of five frequency bands, inter-FU connections between a middle anterior and middle posterior FU are present in the group mean coherence map (Fig. 9) if they are present in the majority of the individual dataset FU maps in the corresponding frequency bands (Figs. 5–8). The only exception is the 8-12 Hz band, with anterior-posterior connections just above the threshold for a majority of three (out of five) younger adults, and with anterior-posterior connections above the threshold for a minority of two (out of five) older adults (with one relatively high value). Thus, generally the common features from the individual FU maps are preserved well in the group mean coherence maps.

2) Group Mean Coherence Map: Comparison Between Groups: For all frequencies (1-30 Hz), the number of FUs is lower for younger than for older adults in the corresponding frequency band (Fig. 9, compare left with right column). This probably corresponds to earlier findings [2], indicating more, especially interhemispheric, coherence for older than for younger adults. Similarly, the number of white cells (corresponding to electrodes not part of any sufficiently large FU) is larger for younger than for older adults in every frequency band, again confirming the presence of more coherence for older than for younger adults [2].

For lower frequencies, there is a connecting line between an anterior and a posterior FU in most group mean coherence maps for younger adults (Fig. 9, 1-7 Hz) and older adults (Fig. 9, 1-

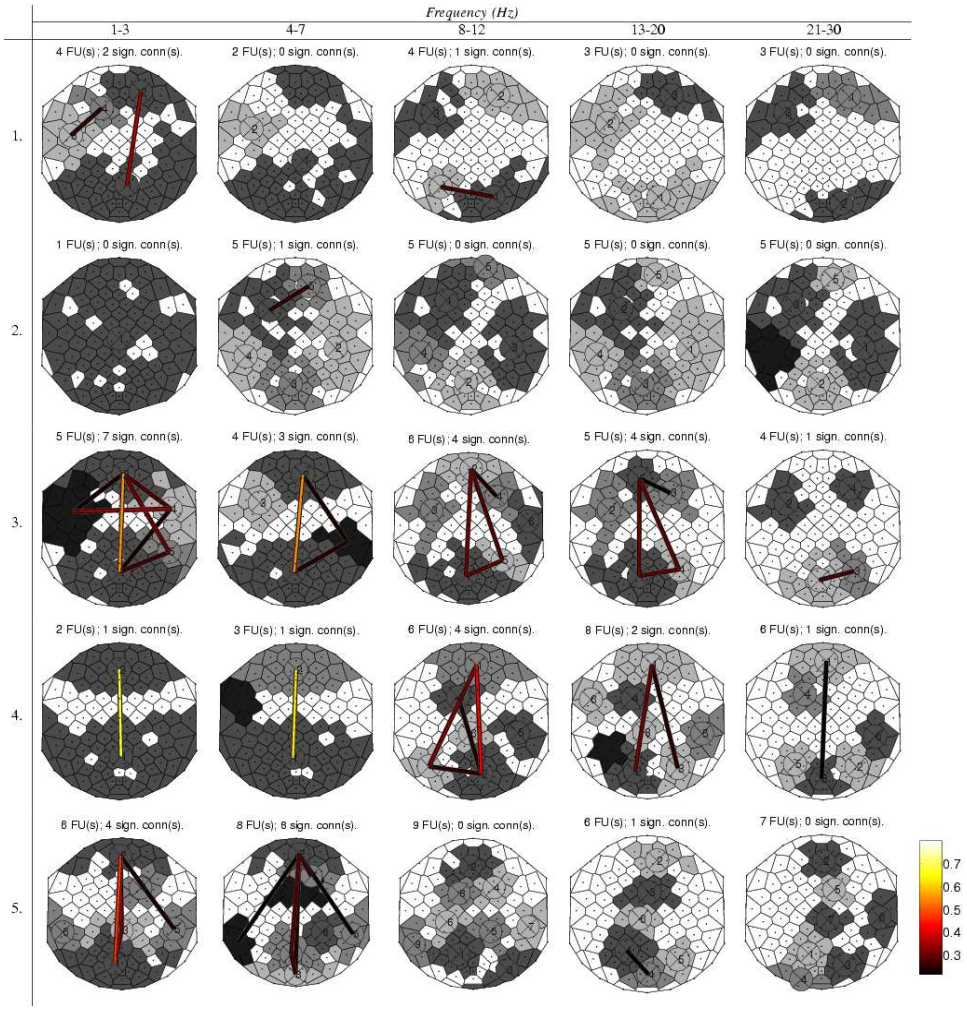

Fig. 6. **Standard MCB FU maps, older adults**. Same parameters as in Fig. 5.

12 Hz). This is possibly associated with the two most important sources of brain activity for this type of experiment, located anteriorly (known as P3a) and posteriorly (known as P3b) [46].

FU maps show more lateral FUs (on both sides of the head) for older adults than for younger adults in the same frequency band (Fig. 9). This may indicate more bilateral activation for older than for younger adults, as was also observed in [2].

3) Group FU Size Map: Comparison Between Groups: For younger adults (Fig. 10, left), average FU sizes are highest in a posterior region and an anterior region, for all frequencies. The lateral regions on both left and right sides have the lowest average FU size.

Similarly, for older adults (Fig. 10, right), the highest average FU sizes occur in a posterior and an anterior region, although for older adults those regions are more widespread than for younger adults. Whereas the average FU sizes are lower on the sides than in the middle for both younger and older adults (Fig. 10), the difference between lower and higher average FU sizes is smaller for older than younger adults. This indicates more bilateral activation for older than younger adults, in correspondence with [2].

Cells for younger adults are generally part of FUs with a lower average size than corresponding cells for older adults (Fig. 10, compare color bars of the left and right column), once more confirming the observation of higher coherence for older than younger adults [2]. Moreover, the average FU size decreases with increasing frequency, in agreement with the presence of simultaneous activity at a more global scale for lower EEG frequencies and at a more local scale for higher EEG frequencies [39].

4) Comparison of Hypothesis-Driven and Data-Driven Approaches: For the same type of data, a hypothesis-driven subselection of 12 out of 119 scalp electrodes (Fp1, Fp2, F3, F4, C3, C4, P3, P4, O1, O2, O3, O4; see Fig. 1, right) and 15 coherences was made [2]. In contrast to this hypothesis-driven approach, FU maps together with group mean coherence maps and group FU size maps all contribute to a data-driven selection of electrodes of interest. In addition to the coherences studied in [2], our data-driven results suggest to include left and right temporal electrodes (e.g., T7 and T8), and to include both intrahemispheric and interhemispheric connections between anterior and posterior regions.

VIII. Discussion and Conclusions

EEG coherence analysis is the study of coherence between functional units. Most current analyses use hypothesis-driven ROIs. Existing data-driven graph visualizations for EEG coherence commonly visualize vertices representing electrodes as dots and coherences as edges, resulting in clutter for multichannel EEG with up to 512 electrodes. However, without a hypothesis, all

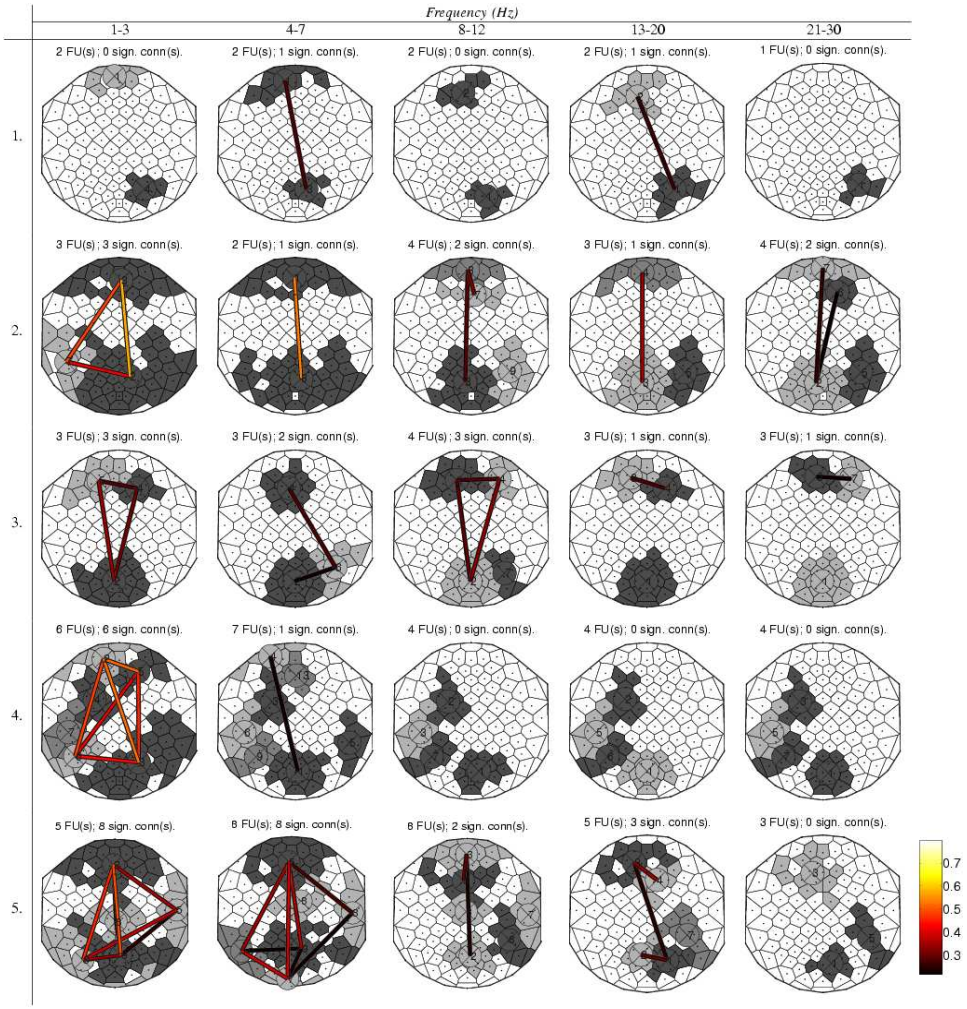

Fig. 7. **Novel IWB FU maps, younger adults.** Same parameters as in Fig. 5

coherences should be considered. Therefore, we presented a data-driven visualization method for multichannel EEG coherence, which strongly reduces clutter and is referred to as functional unit (FU) map. An FU is a spatially connected set of electrodes recording pairwise significantly coherent signals, represented in the graph by a spatially connected clique. The visualization of an FU is a simplified representation of a spatially connected clique which does not explicitly visualize all edges within a clique.

We earlier developed two methods to detect FUs, a maximal clique based (MCB) method (time complexity $O(3^{n/3})$, with n the number of vertices) [20], and a more efficient watershed based (WB) method ($O(n^2 \log n)$) [22]. One of the novelties introduced in this paper is an improved watershed based (IWB) method ($O(n^3)$), merging two spatially neighboring FUs if their union is a clique in the coherence graph. We did not choose one of the common solutions for over-segmentation which uses the concept of dynamics [47], because dynamics are defined for vertex values, whereas the EEG coherence graph has edge values. Moreover, the IWB method merges FUs during segmentation (and not afterwards, such as with hierarchical watersheds [44]). FU detection with the WB and IWB method (taking about 0.04 s and 0.05 s, respectively) is up to a factor of 100,000 faster than the MCB method, and makes interactive visualization of multichannel EEG coherence possible.

The greedy WB and IWB methods directly result in uniquely labeled electrodes, contrary to the standard MCB method. All methods depend on the same thresholds: one for the initial coherence graph, one for the inter-FU coherence, and one for the minimal FU size. The MCB, WB, and IWB methods find FUs in approximately the same locations, and the inter-FU connections present in the MCB FU maps are generally also present in the WB and IWB FU maps. However, the average difference between WB and the MCB method regarding the number of FUs is 1.8 (for the parameters used). For the IWB and the MCB methods the difference has decreased to 0.9, for the case study that was presented here.

Additionally, as an alternative to hypothesis-driven group analysis methods for multichannel EEG coherence, we proposed two novel data-driven group maps for visual group analysis. They are both extensions of the efficient IWB FU detection method. One is a group mean coherence map, which is a data-driven FU map based on the group mean coherence. The other is a group FU size map, showing for each electrode the average FU size across a collection of individual FU maps.

Because conventional data-driven multichannel EEG coherence analysis is cumbersome, comparable conventional findings are rare. Nevertheless several conventional findings are confirmed by observations in the new data-driven visualizations. *(a)* Coherence

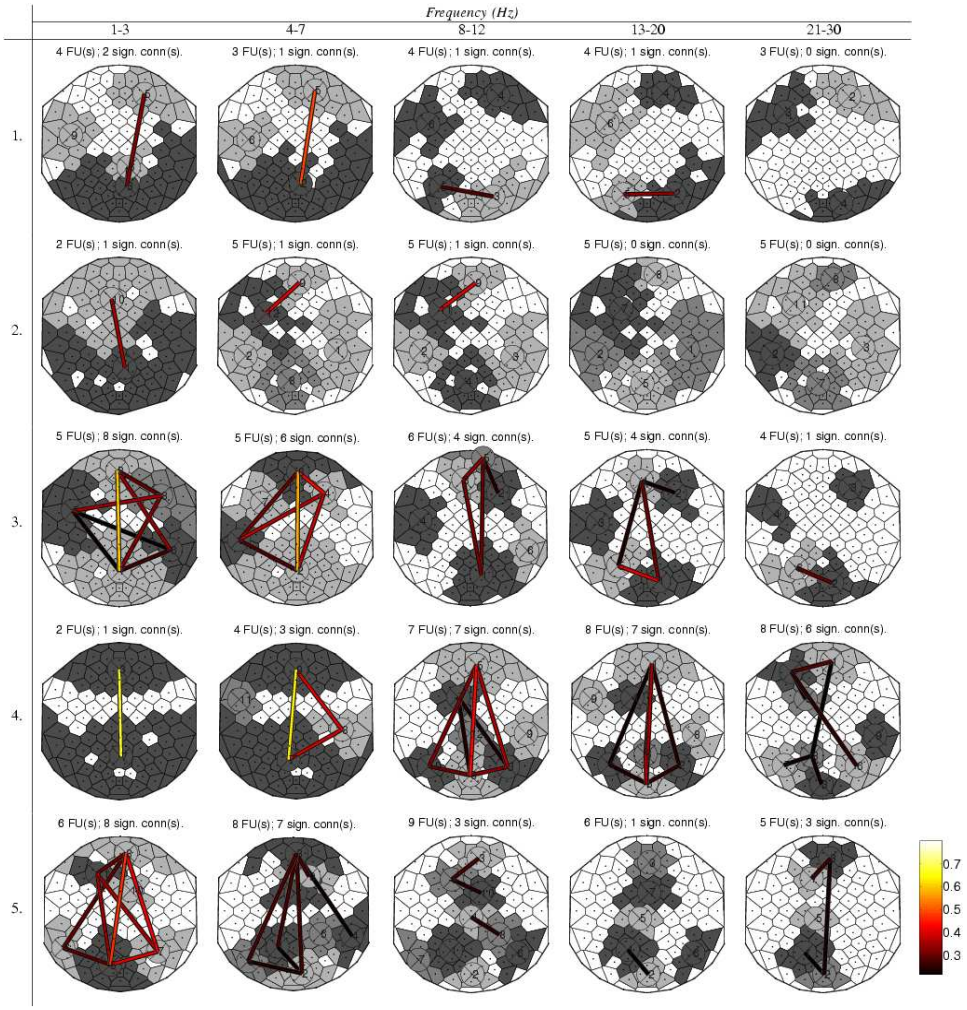

Fig. 8. **Novel IWB FU maps, older adults**. Same parameters as in Fig. 5.

is lower for younger than older adults [2]. Accordingly, the number of FUs in group mean coherence maps is lower for younger than for older adults for 1-30 Hz, group mean coherence maps show a larger number of white cells not part of any sufficiently large FU for younger adults than older adults, and group FU size maps show larger average FU sizes for older than for younger adults. *(b)* Older adults have more bilateral activation than younger adults [2]. Accordingly, for older adults FU maps and group mean coherence maps display more FUs in lateral regions, the average FU size is generally higher and the difference between lower and higher average FU sizes is smaller. *(c)* There is simultaneous activity at a more global scale for lower EEG frequencies and at a more local scale for higher EEG frequencies [39]. Indeed, group FU size maps indicate that the average FU size decreases with increasing frequency. *(d)* The two most important sources of brain activity for this type of data are located anteriorly (known as P3a) and posteriorly (known as P3b) [46]. Accordingly, FU maps and group mean coherence maps show connections between anterior and posterior FUs for lower frequencies.

Thus, the detection of data-driven ROIs for multichannel EEG coherence on the basis of the IWB method results in similar information as the MCB method, and this information is found to agree with conventional findings. Also, the two new data-driven group maps, referred to as group mean coherence map and group FU size map, yield results in accordance with conventional findings. Yet, our results suggest to expand an earlier selection of hypothesis-driven ROIs [2] with additional data-driven ROIs. This demonstrates the usefulness of the IWB FU map, and both new data-driven group maps.

FU maps, group mean coherence maps, and group FU size maps all contribute to a data-driven subselection of electrodes of interest (EOIs): the number of EOIs, their location, and their region of influence can be derived directly from the combination of FU maps, group mean coherence maps, and group FU size maps. In other words, the novel IWB method together with the two new group maps make a data-driven subselection of the available electrophysiological signals possible. This can be used as a data-driven starting point for conventional quantitative group analysis. Our methods are currently applied to a multichannel EEG coherence study of mental fatigue [48] by researchers from the Department of Experimental Psychology of the University of Groningen. In this study, the ROIs are obtained in a data-driven way since no strong hypotheses can be formulated based on existing evidence. Our approach overcomes the severe limitations of conventional hypothesis-driven methods and takes full advantage of all the available recordings. The presented visualization of (group) FU maps provides a very economical data summary

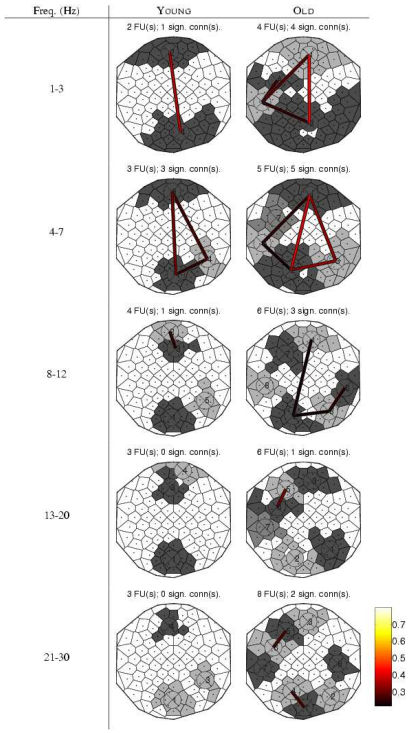

Fig. 9. **Group mean coherence maps** for younger (left) and older (right) adults, per frequency band (from top to bottom). Top view, nose on top. The line color depends on the inter-FU coherence (see color bar, bottom right, with minimum corresponding to the coherence threshold $\phi \approx 0.22$ for $p = 0.01$; the color bar is the same for all FU maps). Above each group mean coherence map, the number of FUs and the number of connecting lines between FUs are displayed.

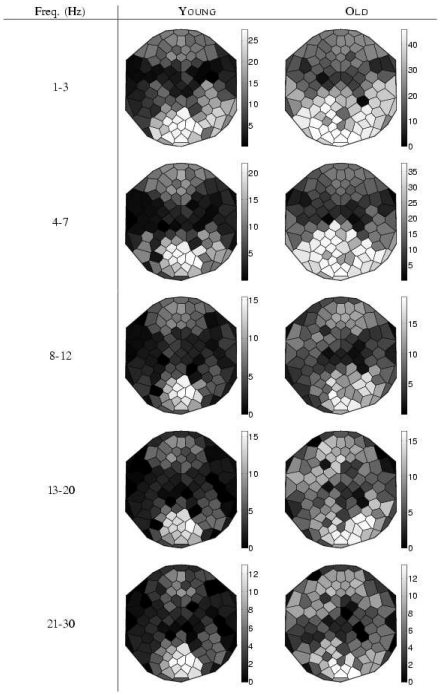

Fig. 10. **Group FU size maps** for younger (left) and older (right) adults, per frequency band (from top to bottom). Top view, nose on top. The average FU size for each electrode, computed for the five individual FU maps of every group (see Fig. 9), is mapped to a gray value (see right bar, with maximum equal to the maximum average FU size). A lighter cell indicates that the corresponding electrode is on average part of larger and more interesting FUs. The gray scale range is adapted per group FU size map, to be able to better distinguish between light and dark regions in one FU size map.

of extensive experimental results, which otherwise would be very difficult and time-consuming to assess. Initial responses from the psychologists using our visualization methods are very favorable.

The IWB method will be available in *FUmaplab* on `http://www.rug.nl/informatica/onderzoek/programmas/svcg/demos`.

References

[1] D. M. Halliday, J. R. Rosenberg, A. M. Amjad, P. Breeze, B. A. Conway, and S. F. Farmer, "A framework for the analysis of mixed time series/point process data - theory and application to the study of physiological tremor, single motor unit discharges and electromyograms," *Prog Biophys Mol Bio*, vol. 64, no. 2/3, pp. 237–278, 1995.

[2] N. M. Maurits, R. Scheeringa, J. H. van der Hoeven, and R. de Jong, "EEG coherence obtained from an auditory oddball task increases with age." *J Clin Neurophysiol*, vol. 23, no. 5, pp. 395–403, 2006.

[3] J. L. W. Bosboom, D. Stoffers, C. J. Stam, B. W. van Dijk, J. Verbunt, H. W. Berendse, and E. C. Wolters, "Resting state oscillatory brain dynamics in Parkinson's disease: An MEG study," *Clin Neurophysiol*, vol. 117, no. 11, pp. 2521–2531, 2006.

[4] Y. Chen, M. Ding, and J. Kelso, "Task-related power and coherence changes in neuromagnetic activity during visuomotor coordination," *Exp Brain Res*, vol. 148, pp. 105–116, 2003.

[5] R. Srinivasan, D. P. Russell, G. M. Edelman, and G. Tononi, "Increased synchronization of neuromagnetic responses during conscious perception," *J Neurosci*, vol. 19, no. 13, pp. 5435–48, 1999.

[6] S. Achard, R. Salvador, B. Whitcher, J. Suckling, and E. Bullmore, "A resilient, low-frequency, small-world human brain functional network with highly connected association cortical hubs," *J Neurosci*, vol. 26, no. 1, pp. 63–72, 2006.

[7] D. Cordes, V. Haughton, J. D. Carew, K. Arfanakis, and K. Maravilla, "Hierarchical clustering to measure connectivity in fMRI resting-state data," *Magn Reson Imaging*, vol. 20, no. 4, pp. 305–17, 2002.

[8] R. Salvador, J. Suckling, C. Schwarzbauer, and E. Bullmore, "Undirected graphs of frequency-dependent functional connectivity in whole brain networks," *Phil T R Soc B*, vol. 360, pp. 937–946, May 2005.

[9] R. Salvador, J. Suckling, M. R. Coleman, D. Pickard, John, D. Menon, and E. Bullmore, "Neurophysiological architecture of functional magnetic resonance images of human brain," *Cereb Cortex*, vol. 15, pp. 1332–1342, September 2005.

[10] M. Kamiński, K. Blinowska, and W. Szelenberger, "Topographic analysis of coherence and propagation of EEG activity during sleep and wakefulness," *Electroen Clin Neuro*, vol. 102, pp. 216–227, 1997.

[11] A. v. Stein, P. Rappelsberger, J. Sarnthein, and H. Petsche, "Synchronization between temporal and parietal cortex during multimodal object processing in man," *Cereb Cortex*, vol. 9, pp. 137–150, 1999.

[12] T. M. J. Fruchterman and E. M. Reingold, "Graph drawing by force-directed placement," *Software - Practice and Experience*, vol. 21, no. 11, pp. 1129–1164, 1991.

[13] N. Wong, S. Carpendale, and S. Greenberg, "EdgeLens: An interactive method for managing edge congestion in graphs," in *Proc. IEEE Symposium on Information Visualization*, 2003, pp. 51–58.

[14] I. Herman, M. S. Marshall, and G. Melancon, "Density functions for visual attributes and effective partitioning in graph visualization," in *Proc. IEEE Symposium on Information Vizualization*. Washington, DC, USA: IEEE Computer Society, 2000, p. 49.

[15] J. Sarnthein, H. Petsche, P. Rappelsberger, G. L. Shaw, and A. von Stein, "Synchronization between prefrontal and posterior association cortex during human working memory." *P Natl Acad Sci USA*, vol. 95, no. 12, pp. 7092–6, 1998.

[16] T. E. Gladwin, J. P. Lindsen, and R. de Jong, "Pre-stimulus EEG effects related to response speed, task switching and upcoming response hand." *Biol Psychol*, vol. 72, no. 1, pp. 15–34, 2006.

[17] P. J. Franaszczuk, G. K. Bergey, and M. J. Kamiński, "Analysis of mesial temporal seizure onset and propagation using the directed transfer function method." *Electroen Clin Neuro*, vol. 91, no. 6, pp. 413–27, 1994.

[18] M. ten Caat, N. M. Maurits, and J. B. T. M. Roerdink, "Tiled parallel coordinates for the visualization of time-varying multichannel EEG data,"

in *Proc. Eurographics/IEEE VGTC Symposium on Data Visualization (EuroVis)*, 2005, pp. 61–68.
[19] M. ten Caat, N. M. Maurits, and J. B. T. M. Roerdink, "Design and evaluation of tiled parallel coordinate visualization of multichannel EEG data," *IEEE T Vis Comput Gr*, vol. 13, no. 1, pp. 70–79, 2007.
[20] M. ten Caat, N. M. Maurits, and J. B. T. M. Roerdink, "Functional unit maps for data-driven visualization of high-density EEG coherence," in *Proc. Eurographics/IEEE VGTC Symposium on Visualization (EuroVis)*, 2007, pp. 259–266.
[21] J. P. Lachaux, E. Rodriguez, J. Martinerie, and F. J. Varela, "Measuring phase synchrony in brain signals." *Hum Brain Mapp*, vol. 8, no. 4, pp. 194–208, 1999.
[22] M. ten Caat, N. M. Maurits, and J. B. T. M. Roerdink, "Watershed-based visualization of high-density EEG coherence," in *Proc. 8th International Symposium on Mathematical Morphology, Rio de Janeiro*, G. J. F. Banon, J. Barrera, and U. de Mendoca Braga-Neto, Eds., Oct 10-13 2007, pp. 289–300.
[23] M. G. Knyazeva, E. Fornari, R. Meuli, and P. Maeder, "Interhemispheric integration at different spatial scales: the evidence from EEG coherence and fMRI." *J. Neurophysiol.*, vol. 96, no. 1, pp. 259–75, 2006.
[24] E. Pereda, R. Q. Quiroga, and J. Bhattacharya, "Nonlinear multivariate analysis of neurophysiological signals." *Prog Neurobiol*, vol. 77, no. 1-2, pp. 1–37, 2005.
[25] B. Horwitz, "The elusive concept of brain connectivity." *Neuroimage*, vol. 19, no. 2 Pt 1, pp. 466–70, 2003.
[26] G. Tononi and G. M. Edelman, "Consciousness and complexity." *Science*, vol. 282, no. 5395, pp. 1846–51, 1998.
[27] D. Archambault, T. Munzner, and D. Auber, "Smashing peacocks further: Drawing quasi-trees from biconnected components," *IEEE T Vis Comput Gr (Proc. Vis/InfoVis 2006)*, vol. 12, no. 5, pp. 813–820, September-October 2006.
[28] Y. Chiricota, F. Jourdan, and G. Melancon, "Software components capture using graph clustering," in *Proc. EEE International Workshop on Program Comprehension*, 2003, p. 217.
[29] A. Delorme, S. Makeig, M. Fabre-Thorpe, and T. Sejnowski, "From single-trial EEG to brain area dynamics," *Neurocomputing*, vol. 44–46, pp. 1057–1064, 2002.
[30] S. Makeig, A. Delorme, M. Westerfield, T.-P. Jung, J. Townsend, E. Courchesne, and T. J. Sejnowski, "Electroencephalographic brain dynamics following manually responded visual targets." *PLoS Biol*, vol. 2, no. 6, pp. 747–62, 2004.
[31] F. De Vico Fallani, L. Astolfi, F. Cincotti, D. Mattia, A. Tocci, M. Grazia Marciani, A. Colosimo, S. Salinari, S. Gao, A. Cichocki, and F. Babiloni, "Extracting information from cortical connectivity patterns estimated from high resolution EEG recordings: A theoretical graph approach." *Brain Topogr*, vol. 19, no. 3, pp. 125–136, 2007.
[32] R. Srinivasan, "Methods to improve the spatial resulution of EEG," *Int J of Bioelectromagnetism*, vol. 1, no. 1, 1999.
[33] P. Rappelsberger and H. Petsche, "Probability mapping: power and coherence analyses of cognitive processes." *Brain Topogr*, vol. 1, no. 1, pp. 46–54, 1988.
[34] B. Schack, A. C. Chen, S. Mescha, and H. Witte, "Instantaneous EEG coherence analysis during the Stroop task." *Clin Neurophysiol*, vol. 110, no. 8, pp. 1410–26, 1999.
[35] G. Nolte, O. Bai, L. Wheaton, Z. Mari, S. Vorbach, and M. Hallett, "Identifying true brain interaction from EEG data using the imaginary part of coherency." *Clin Neurophysiol*, vol. 115, no. 10, pp. 2292–307, 2004.
[36] K. J. Worsley, J.-I. Chen, J. Lerch, and A. C. Evans, "Comparing functional connectivity via thresholding correlations and singular value decomposition." *Philos T Roy Soc B*, vol. 360, no. 1457, pp. 913–20, 2005.
[37] V. G. van de Ven, E. Formisano, D. Prvulovic, C. H. Roeder, and D. E. J. Linden, "Functional connectivity as revealed by spatial independent component analysis of fMRI measurements during rest." *Hum Brain Mapp*, vol. 22, no. 3, pp. 165–78, 2004.
[38] F. T. Sun, L. M. Miller, and M. D'Esposito, "Measuring interregional functional connectivity using coherence and partial coherence analyses of fMRI data," *NeuroImage*, vol. 21, pp. 647–658, 2004.
[39] P. L. Nunez, R. Srinivasan, A. F. Westdorp, R. S. Wijesinghe, D. M. Tucker, R. B. Silberstein, and P. J. Cadusch, "EEG coherency. I: Statistics, reference electrode, volume conduction, Laplacians, cortical imaging, and interpretation at multiple scales." *Electroen Clin Neuro*, vol. 103, no. 5, pp. 499–515, 1997.
[40] C. Bron and J. Kerbosch, "Algorithm 457: finding all cliques of an undirected graph," *Commun ACM*, vol. 16, no. 9, pp. 575–577, 1973.
[41] E. Tomita, A. Tanaka, and H. Takahashi, "The worst-case time complexity for generating all maximal cliques and computational experiments," *Theor Comput Sci*, vol. 363, no. 1, pp. 28–42, 2006.
[42] J. B. T. M. Roerdink and A. Meijster, "The watershed transform: definitions, algorithms, and parallellization strategies," *Fundamenta Informaticae*, vol. 41, pp. 187–228, 2000.
[43] D. R. Wood, "An algorithm for finding a maximum clique in a graph," *Oper Res Lett*, vol. 21, no. 5, pp. 211–217, 1997.
[44] T. Schultz, H. Theisel, and H.-P. Seidel, "Segmentation of DT-MRI anisotropy isosurfaces," in *Proc. Eurographics/IEEE VGTC Symposium on Visualization (EuroVis)*, K. Museth, T. Möller, and A. Ynnerman, Eds. Eurographics, 2007, pp. 187–194.
[45] S. Beucher and F. Meyer, "The morphological approach to segmentation: the watershed transformation," in *Mathematical Morphology in Image Processing*, E. Doherty, Ed. New York: Marcel Dekker, 1993, ch. 12, pp. 433–481.
[46] M. D. Comerchero and J. Polich, "P3a and P3b from typical auditory and visual stimuli," *Clin Neurophysiol*, vol. 110, no. 1, pp. 24–30, 1999.
[47] M. Grimaud, "A new measure of contrast: dynamics," in *Proc. SPIE Image Algebra and Morphological Processing III*, vol. 1769, 1992, pp. 292–305.
[48] M. ten Caat, M. M. Lorist, E. Bezdan, J. B. T. M. Roerdink, and N. M. Maurits, "High-density EEG coherence analysis using functional units applied to a mental fatigue study," *J Neurosci Meth*, 2007, submitted.

Michael ten Caat obtained his M.Eng. in applied mathematics (2002) and his M.Sc. in numerical mathematics (2003) from the University of Groningen, The Netherlands. He currently is a PhD candidate in the research group of Scientific Visualization and Computer Graphics at the department of Mathematics and Computing Science, University of Groningen. His research interests include scientific visualization and information visualization, in particular applied to medical applications.

Natasha M. Maurits received her M.Eng. ('94) in applied mathematics, her M.Sc. ('94) in numerical mathematics and her Ph.D. ('98) in Chemistry, from the University of Groningen, the Netherlands. She is currently associate professor in biomedical signal analysis with a special interest in clinical neurophysiology, in the department of Neurology of the University Medical Center Groningen. Her research interests include computational fluid dynamics models of the vascular circulation, analysis and clinical applications of multi-channel EEG and simultaneous EEG/EMG/fMRI recordings.

Jos B. T. M. Roerdink received his M.Sc. (1979) in theoretical physics from the University of Nijmegen, the Netherlands. Following his Ph.D. (1983) from the University of Utrecht and a two-year position (1983-1985) as a Postdoctoral Fellow at the University of California, San Diego, both in the area of stochastic processes, he joined the Centre for Mathematics and Computer Science in Amsterdam. There he worked from 1986-1992 on image processing and tomographic reconstruction. He is currently full professor of Scientific Visualization and Computer Graphics at the Institute for Mathematics and Computing Science of the University of Groningen, The Netherlands. His research interests include mathematical morphology, biomedical visualization, neuroimaging and bioinformatics.